Ion dynamics and oscillation frequencies in a linear combined trap

T. Nakamura[a] and S. Ohtani
Institute for Laser Science, University of Electro-Communications, 1-5-1 Chofugaoka, Chofu, Tokyo 182-8585, Japan

M. Wada[b]
Institute of Physical and Chemical Research (RIKEN), 2-1 Hirosawa, Wako, Saitama 351-0198, Japan

K. Okada
Department of Physics, Sophia University, 7-1 Kioicho, Chiyoda, Tokyo 102-8554, Japan

I. Katayama
Institute of Particle and Nuclear study (IPNS), High Energy Accelerator Research Organization (KEK), 1-1 Oho, Tsukuba, Ibaraki 305-0801, Japan

H. A. Schuessler
Department of Physics, Texas A & M University, College Station, Texas 77843

(Received 24 August 2000; accepted for publication 4 December 2000)

Ion traps have been pivotal in opening new frontiers for the precision spectroscopy of stable ions. We report on the demonstration of an additional ion trap: the linear combined trap. This device is particularly well suited for trapping ions with unstable nuclei, due to its large range of stability parameters that facilitates external injection online to an accelerator. The motion of an ion in such a linear combined trap is investigated theoretically and experimentally. In the trap ions oscillate harmonically in the radial direction and move nearly harmonically between fixed boundaries along the longitudinal axis. The presence of a homogeneous magnetic field and the applied dc and rf electric fields, lead to a set of coupled Mathieu equations. Their approximate solutions exhibit motional frequencies, which are combinations of shifted macromotion frequencies and the cyclotron frequency. The dependence of these motional frequencies on the applied trapping fields was studied in detail. For the measurements we used small clouds of laser cooled $^9Be^+$ ions and crystallized $^9Be^+$ ions. The observed oscillation frequencies are compared to both the results of zeroth order analytical solutions and to numerical simulations in which the frequency spectrum was obtained from the ion orbits by using the fast fourier transform formalism. The various motional resonances were experimentally recorded by applying a weak dipole excitation field to one of the trap electrodes, and by simultaneously observing at resonance the changes in the fluorescence intensity. Depending on the detuning of the cooling laser the ions gain energy during the motional excitation process in such a way that they are shifted further in or out of optical resonance by the Doppler effect. This leads to either positive or negative ion motion signals at the various ion oscillation frequencies. © *2001 American Institute of Physics.* [DOI: 10.1063/1.1345514]

I. INTRODUCTION

In a combined trap we can store charged particles by superposing time-independent dc and oscillatory quadrupole potentials onto a homogeneous magnetic field. Such a combined trap can be considered to be a rf trap[1–4] and a Penning trap[5–7] in a single device. The symmetrical combined trap has been known for some time.[8–13] In it the ions move in a three-dimensional potential well. However, following the recent developments of linear traps[14,15] we have proposed[16] and built a linear combined trap. In this article measurements of the characteristics of the ion oscillation frequencies performed for this device are presented. In addition we derive an approximate theory that analytically describes the ion dynamics. The linear geometry provides a long potential valley, which is harmonic along the *x, y* directions, and near harmonically closed on both ends at suitably chosen distances along the *z* axis. In this way the linear trap is the ideal device for laser cooling many stored ions simultaneously, so that at low densities they arrange themselves in single file along the axis of the trap at the bottom of the potential valley.[17,18] The combined trap has all the features of the rf and Penning traps, and, in addition, the possibility to simultaneously store particles with a large mass difference. When reducing either the magnetic field or the rf and dc electric fields the combined trap can be transformed into a pure rf trap or a Penning trap-like device.

Our main application of the linear combined trap is to make a precise measurement of the nuclear magnetic moments of the various isotopes of Be^+ ions by laser-rf triple resonance spectroscopy.[19,20] These measurements will be described in a forthcoming article. For high accuracy a strong magnetic field is required.[21,22] For such measurements the combined trap is superior to the Penning trap due to the

[a]Present address: Institute of Physical and Chemical Research (RIKEN).
[b]Electronic mail: mw@riken.go.jp

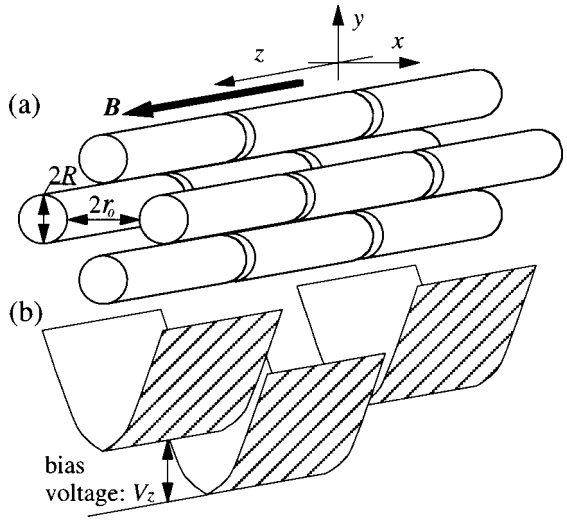

FIG. 1. Schematic diagram of a linear combined trap. (a) Three sets of four circular ion trap electrodes are placed in a magnetic field which is oriented parallel to the trap electrodes. (b) The trapping field potentials with the storage section in the middle are shown.

better signal to noise ratio as a consequence of the possible strong concentration of the cooled ions along the trap axis. Also, external injection is favored for the combined trap since it has a larger stability region than other storage devices. The combined trap also has ideal geometrical matching and good coupling for an upstream ion beam guide by which radioactive ions can be transported to the trap from an isotope separator.[23] This is particularly useful when radioactive ions produced online at a nuclear accelerator[24] need to be studied. In this context, the nuclear moments, as well as their distributions in a nucleus, can be determined.[25]

This article is divided into seven parts. After the introduction we find in Sec. II an approximate analytical solution for the equations of motion of ions stored in a linear combined trap using a set of coupled Mathieu equations. Next, in the experimental section we described the apparatus and the measurement procedure using cooled clouds of ions and crystallized ions. In Sec. IV the observation of the various ion oscillation frequencies and their dependence on the operational parameters are given. Section V presents the numerical simulation of the ion dynamics. Here the fast Fourier transform (FFT) formalism yields the ion oscillation frequencies from the calculated ion orbits. In Sec. VI we compare the results of the measurements with theory and the simulations, and discuss the occurrence of spurious motional resonances. Finally, the different modes of the trap operation are related to each other in Sec. VII.

II. THEORY

A. Ion motion

Figure 1 displays the geometrical arrangement and segmentation of a linear combined trap into three sections, which carry the same rf voltage, but which can be individually biased to restrict the motion of the ions along the trap axis in the center section. The basic equation of motion of a charged particle of mass m and charge e in the trap is

$$m\ddot{\mathbf{r}} = -e\nabla\Phi + e\dot{\mathbf{r}}\times\mathbf{B}. \tag{1}$$

The ions move under the influence of a magnetic field $\mathbf{B}$ and an electric field $-\nabla\Phi$. The electric field is produced by applying the voltage $\Phi_0(t) = V_{\mathrm{dc}} - V_{\mathrm{ac}}\cos\Omega t$ between the adjacent electrodes of four cylindrical electrodes and the bias voltage V_z. In the region near the midpoint of the trap axis, the potential Φ can be approximated

$$\Phi(x,y,z,t) = \Phi_0(t)\frac{x^2-y^2}{2r_0^2} + \frac{\alpha V_z}{z_0^2}\left(z^2 - \frac{x^2+y^2}{2}\right). \tag{2}$$

Here $2r_0$ is the separation of opposite electrodes, z_0 is half the length of the central region, and α is a geometric factor of the trap. The magnetic field $\mathbf{B}$ is homogeneous and oriented along the z axis according to $\mathbf{B}=(0,0,B_0)$. In this way the Lorentz force provides additional radial confinement.

The equation of motion of an ion is

$$\begin{aligned}
\ddot{x} &= -\frac{e}{mr_0^2}(V_{\mathrm{dc}} - V_{\mathrm{ac}}\cos\Omega t)x + \frac{e\alpha V_z}{mz_0^2}x + \frac{eB_0}{m}\dot{y},\\
\ddot{y} &= \frac{e}{mr_0^2}(V_{\mathrm{dc}} - V_{\mathrm{ac}}\cos\Omega t)y + \frac{e\alpha V_z}{mz_0^2}y - \frac{eB_0}{m}\dot{x},\\
\ddot{z} &= -\frac{2e\alpha V_z}{mz_0^2}z.
\end{aligned} \tag{3}$$

The z equation describes the simple harmonic motion along the longitudinal z axis. In the transverse x and y directions the ions are harmonically bound. The motional equations can be rewritten in the form of coupled Mathieu differential equations

$$\begin{aligned}
&\frac{d^2x}{d\tau^2} + \left(a - \frac{b}{2} - 2q\cos 2\tau\right)x - 2g\frac{dy}{d\tau} = 0,\\
&\frac{d^2y}{d\tau^2} - \left(a + \frac{b}{2} - 2q\cos 2\tau\right)y + 2g\frac{dx}{d\tau} = 0,\\
&\frac{d^2z}{d\tau^2} + bz = 0,
\end{aligned} \tag{4}$$

with the dimensionless parameters

$$\begin{aligned}
&\tau = \frac{1}{2}\Omega t, \quad a = \frac{4eV_{\mathrm{dc}}}{m\Omega^2 r_0^2}, \quad q = \frac{2eV_{\mathrm{ac}}}{m\Omega^2 r_0^2},\\
&b = \frac{8e\alpha V_z}{m\Omega^2 z_0^2}, \quad \omega_c = \frac{eB_0}{m}, \quad g = \frac{\omega_c}{\Omega}.
\end{aligned} \tag{5}$$

The equation along the z axis is independent from the transverse motion and can be solved separately

$$\begin{aligned}
z &= Z_1\exp(i\sqrt{b}\tau) + Z_2\exp(-i\sqrt{b}\tau)\\
&= Z_1\exp(i\omega_z t) + Z_2\exp(-i\omega_z t),
\end{aligned} \tag{6}$$

where the z motion frequency is given by

$$\omega_z = \frac{\sqrt{b}\Omega}{2} = \sqrt{\frac{2e\alpha V_z}{mz_0^2}}. \tag{7}$$

In the special case that $a=g=b=0$ and $q\neq 0$, the equations along the transverse directions reduce to the uncoupled Mathieu equations; the solution of which is the well-known secular oscillation of the ion motion[26]

$$x(\tau)=\sum_{n=-\infty}^{\infty} x_n(\tau)=A_0\sum_n C_{2n}\exp[i(\beta_0+2n)\tau] + A_0'\sum_n C_{2n}\exp[-i(\beta_0+2n)\tau],$$
$$y(\tau)=\sum_{n=-\infty}^{\infty} y_n(\tau)=B_0\sum_n C_{2n}\exp[i(\beta_0+2n)\tau] + B_0'\sum_n C_{2n}\exp[-i(\beta_0+2n)\tau], \tag{8}$$

with $\beta_0\simeq\sqrt{q^2/2}$. For the zeroth order approximation of Eq. (4), if $a=g=b=0$ we replace the secular motion by harmonic dynamics in the pseudopotential[3] according to

$$\frac{d^2x}{d\tau^2}=+(2q\cos 2\tau)x\simeq-\beta_0^2x,$$
$$\frac{d^2y}{d\tau^2}=-(2q\cos 2\tau)y\simeq-\beta_0^2y, \tag{9}$$

yielding when β_0 is inserted into Eq. (4)

$$\frac{d^2x}{d\tau^2}+\left(\beta_0^2+a-\frac{b}{2}\right)x-2g\frac{dy}{d\tau}=0,$$
$$\frac{d^2y}{d\tau^2}+\left(\beta_0^2-a-\frac{b}{2}\right)y+2g\frac{dx}{d\tau}=0. \tag{10}$$

Assuming that the solutions have the form

$$x=A\exp(i\beta\tau)\quad\text{and}\quad y=B\exp(i\beta\tau). \tag{11}$$

and substituting above, we obtain

$$\begin{bmatrix}-\beta^2+\beta_0^2+a-b/2 & -i2g\beta\\ +i2g\beta & -\beta^2+\beta_0^2-a-b/2\end{bmatrix}\begin{bmatrix}A\\B\end{bmatrix}=0. \tag{12}$$

The characteristic equation of this matrix can be solved and is given by

$$\beta^2=\beta_0^2-\frac{b}{2}+2g^2\pm\sqrt{4g^2\left(\beta_0^2-\frac{b}{2}+g^2\right)+a^2}$$
$$\simeq\frac{q^2}{2}-\frac{b}{2}+2g^2\pm\sqrt{2g^2(q^2-b+2g^2)+a^2}. \tag{13}$$

Substitution of Eq. (13) into Eq. (11) yields the x and y coordinates of an ion orbit and two motional frequencies. We label these frequencies ω_h (high) and ω_l (low). It follows

$$\omega_{h,l}=\frac{\beta\Omega}{2}=\left[\omega_0^2-\frac{\omega_z^2}{2}+\frac{\omega_c^2}{2}\pm\sqrt{\omega_c^2\left(\omega_0^2-\frac{\omega_z^2}{2}+\frac{\omega_c^2}{4}\right)+\omega_a^4}\right]^{1/2} \tag{14}$$

with

$$\omega_0=\frac{\beta_0\Omega}{2}\simeq\sqrt{\frac{q^2}{2}}\frac{\Omega}{2},\quad \omega_a=\frac{\sqrt{|a|}\Omega}{2}. \tag{15}$$

Note that when the trap is operated without magnetic field, these frequencies become

$$\omega_{h,l}^0\simeq\left(\frac{q^2}{2}-\frac{b}{2}\pm|a|\right)^{1/2}\frac{\Omega}{2}=\sqrt{\omega_0^2-\frac{\omega_z^2}{2}\pm\omega_a^2} \tag{16}$$

which are the characteristic frequencies of the linear rf trap. From the form of these frequencies we obtain the stability condition to be

$$\omega_0>\sqrt{\omega_z^2/2+\omega_a^2}. \tag{17}$$

In the other extreme case, when the trap is operated without rf, but with a magnetic field and a dc-electric field along the z direction we obtain

$$\omega_{h,l}=\left(\frac{\omega_c^2}{2}-\frac{\omega_z^2}{2}\pm\sqrt{\frac{\omega_c^4}{4}-\frac{\omega_c^2\omega_z^2}{2}+\omega_a^4}\right)^{1/2}, \tag{18}$$

where ω_h is the modified cyclotron frequency and ω_l is the modified magnetron frequency. In general the combined trap is stable for all values of ω_h. For ω_l there exist an instability region when

$$\sqrt{\omega_z^2/2-\omega_\alpha^2}<\omega_0<\sqrt{\omega_z^2/2+\omega_a^2}. \tag{19}$$

In this instability region the rotational direction of ω_l is inverted and it then corresponds to the magnetron motion of the Penning trap.

III. EXPERIMENTAL ARRANGEMENT

A. Apparatus

A diagram of the apparatus is shown in Fig. 2. It illustrates as the major parts the linear trap electrodes, the superconducting Helmholtz magnet, and a position resolving photon counting camera. The mechanical construction of the linear trap is similar to that of a quadrupole mass filter. The four quadrupole electrodes are made of cylindrical nonmagnetic stainless steel rods with a diameter $2R=6$ mm. The ratio of the rod diameter to the diagonal separation of opposite electrodes $2r_0$ was chosen to be $2R/2r_0=1.15$.[27] This choice minimizes anharmonicity contributions to the field in the vicinity of the trap center.

In the present experiment the trap consisted of four rather than three segments. Trap operation and the manipulation of the stored ions are depicted in Fig. 3. The trap was operated in the unbalanced mode for ease in applying the various ion motion excitation voltages. In the unbalanced mode the rf voltage is applied only to one pair of electrodes whereas the other pair is grounded [Fig. 3(a)]. The rf-driving frequency $\Omega/2\pi$ was about 7 MHz. The rf amplitude $V_{\rm ac}$ and dc quadrupole voltages $V_{\rm ac}$ were varied over a wide range of values to systematically measure the effect of changing the operating voltages on the ion motion frequencies. The outer two segments (length 15 mm) are positively biased by V_{z1} to produce the longitudinal closing field of the trap. The two inner segments (length 20 mm) are used for loading the trap with ions. The ions are then accumulated for observation of

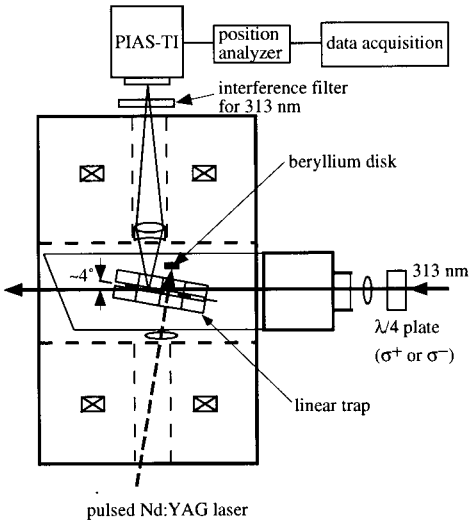

FIG. 2. Experimental apparatus used for fluorescence probing of the ion motion resonances. The four section combined trap is mounted in a superconducting magnet. A room-temperature bore offers access for the pulsed ablation laser and the cw circularly polarized cooling laser. A position-sensitive photon counting camera records the signal.

the ion fluorescence in the measurement section by a suitably applied bias voltage V_{z2}. The trap is filled with $^9Be^+$ ions (natural isotopic abundance 100%) by evaporating and ionizing Be atoms with a pulsed YAG laser (with an energy of 15 mJ/pulse and a pulse duration of 6 ns) from a beryllium disk located next to the central loading section. For dipole excitation of the motional frequencies, a small excitation rf voltage, $V_s \cos 2\pi f_s t$, was applied to one of the ion trap electrodes where V_s was about 0.01 V.

The maximum field of the superconducting magnet was 1 T. The magnetic field was calibrated with a small nuclear magnetic resonance probe. The magnetic field homogeneity over the region of the trapped ions of about 1 mm^3 was $|\Delta B/B| = 5 \times 10^{-7}$. Since the bore in the magnet was at room temperature, it enabled us to insert and retract the glass tube containing the ion trap at all times.

A beam of single frequency tunable laser radiation of typically 100 μW power was focused to a waist of about 100 μm at the location of the ions. For our experiments the strong resonance transition from the $2^2S_{1/2}$ ground state to the $2^2P_{3/2}$ excited state with radiation at $\lambda = 313$ nm was employed. A partial energy level diagram of $^9Be^+$ is depicted in Fig. 4. In this diagram the hyperfine structure splitting (HFS) is neglected. For cooling, the laser frequency was slightly red detuned and either σ^- or σ^+ radiation was used. A small angle of about 4° between the laser beam and the trap axis was chosen to efficiently remove energy from all degrees of freedom of the ion cloud and to produce few ion crystals. The sensitivity was such that the motional resonances of single ions could be observed. The ion fluorescence was imaged by a combination of achromatic lenses through a side hole in the superconducting magnet onto the cathode of a position resolved single photon counting camera (Hamamatsu type PIAS-TI).

B. Measurement procedure

All measurements of the ion motion spectrum were carried out on laser cooled ions, although some spectra are obtained on ion clouds, others on ion crystals. The motional state of the ions was dependent on the laser detuning δ, the power of the cooling laser, and the number of ions in the trap. Figure 5 displays a sequence of fluorescence spectra as a function of laser detuning δ. For each scan, the number of stored ions is different and decreases from trace (a) to (c). For a small enough ion cloud (typically less than 100 ions) the spectrum exhibits the characteristic phase transition from a cloud state to a crystalline state. The wide structures on the left (a), (b), and (c) represent cloud spectra, while the high peak on the right of (c) indicates the spectrum of an ion

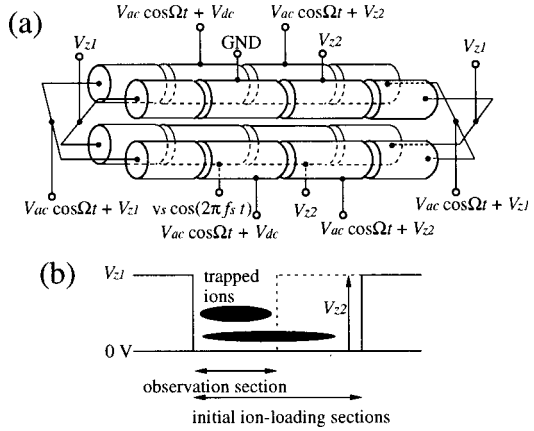

FIG. 3. Ion trap operation: (a) The voltages applied to diagonally located pairs of electrodes are shown for the unbalanced trap operation mode. (b) Procedure for loading ions. Different dc-bias voltages applied to the four trap sections are depicted. The ion cloud trapped after the initial loading is for a measurement compressed to the observation section by switching the voltage on the second section positive. This procedure minimized contact potential problems by beryllium deposition after laser ablation.

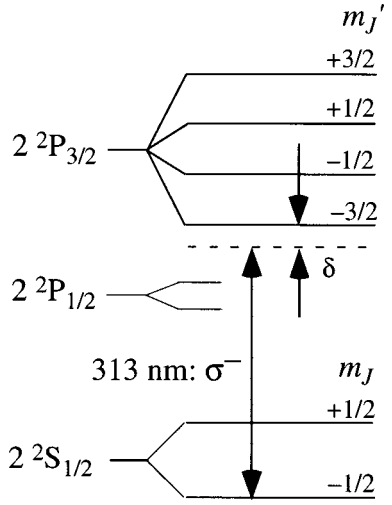

FIG. 4. Partial energy level diagram of $^9Be^+$ in strong magnetic field (HFS neglected), showing the recyclable σ^- transition used for laser cooling. A corresponding σ^+ transition between the $m_J = +1/2$ and $m_J' = +3/2$ can also be employed.

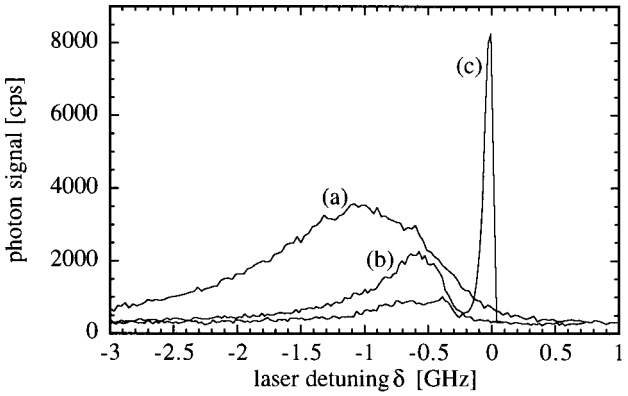

FIG. 5. Fluorescence spectra of stored $^9Be^+$ ions obtained by sweeping the red detuned laser into resonance. The changing parameter is the number of stored ions. Cooled clouds containing several hundred ions produce spectra (a) and (b). The phase transition to the crystalline state (c) is evident by the narrow peak. In this case the cloud contains only a few tens of ions.

crystal. The minimum between the two kinds of spectra corresponds to the phase transition, where the disordered cloud state changes instantaneously to the ordered crystalline state. For the example shown, the peak intensity of the fluorescence in the crystal state is about ten times the peak intensity in the cloud state.

Next the ion motion frequencies were excited by sweeping an additional rf driving field through resonance. The driving voltage was applied to one central trap electrode. For these measurements, the dipole mode of excitation was used. Figure 6(a) shows the location of the various ion motion resonances and their dependence on the magnetic field. Depending on the value of the magnetic field, one major resonance namely f_h shifts to higher oscillation frequencies, whereas the other one, f_l, shifts to lower ones ($f_{h,l} = \omega_{h,l}/2\pi$). Depending on the detuning δ and temperature of the ions, the observed changes in fluorescence intensity are either negative or positive. In a typical experiment, after loading the trap with a large number of ions the laser is initially detuned by about 700 MHz to the red side of the resonance. In this case, a cloud spectrum is observed. When the ions are resonantly heated by driving their macromotion, the cloud both expands and becomes detuned by the increasing Doppler width. This causes the fluorescence to decrease and a motional resonance is observed as a dip. It should be noted that, in general, the ions are not lost in this process since the fluorescence returns to the same level as it had before the motional resonance was excited. Outside a motional resonance the damping of the ion motion by the red detuned laser forces the cloud back to the original cooled state. While taking the various sequences, care was taken to ensure that the magnetic field of the superconducting magnet had stabilized before the next measurement was carried out. All spectra were observed during one measurement cycle over a time period of about 10 h. During this time, a few ion loadings were carried out. Only the number of stored ions changes decreasing from several hundred in the top traces to just a few ions in the bottom traces. To take the measurements on just a few ions (last few traces), the laser detuning

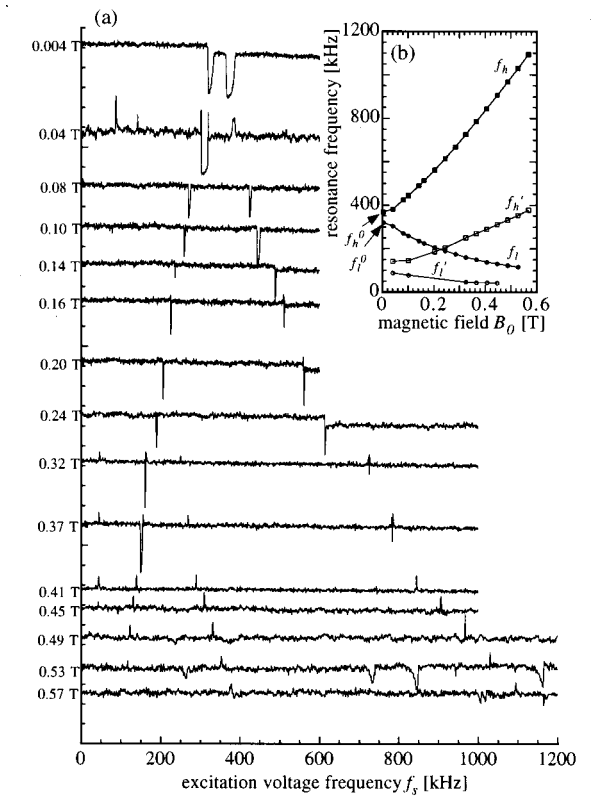

FIG. 6. (a) Sequences of ion oscillation frequencies. Mainly motional spectra of $^9Be^+$ ions but also a few background ions ($M=27$) were registered for increasing magnetic field. The insert (b) depicts this dependence in a graphical form and the measured resonance frequencies are plotted. ($V_{ac}^{app} = 100$ V, $V_{dc}^{app}=0$, $\Omega/2\pi=7.30$ MHz, $V_z^{app}=5$ V.)

was reduced to be only 200 MHz towards the red side. At this value an ion crystal just beyond the phase transition point having only weak fluorescence was produced. In this situation, resonant heating at a macromotion frequency transforms the ion crystal to a cloud state which has a higher fluorescence intensity and a fluorescence peak indicates the motional resonance.

IV. EXPERIMENTAL RESULTS

The measured magnetic field dependence of f_h and f_l is plotted in the Fig. 6(b). The data was compiled from measurements such as shown in Fig. 6(a). At times some additional weak resonance signals appear in the spectra. Although they display a similar field dependence, they are at different frequencies than the $^9Be^+$ resonance. (We will discuss the origin of these spurious resonances in Sec. VI C.)

The applied trap operation parameters were $\Omega/2\pi = 7.30$ MHz, $V_{ac}^{app}=100$ V, $V_{dc}^{app}=0$. For the present unbalanced mode of applying the driving voltages, we had to use voltages with respect to the trap center, and also effective voltages V_{ac} and V_{dc}. The effective voltages are the values seen by the stored ions and are slightly different from the applied voltages. The distinction is necessary for V_{ac} due to the use of circular and nonhyperbolic shaped trap electrodes as required by theory. The effective V_{dc} is the sum of applied V_{dc}^{app} and a small correction. This correction is the contact

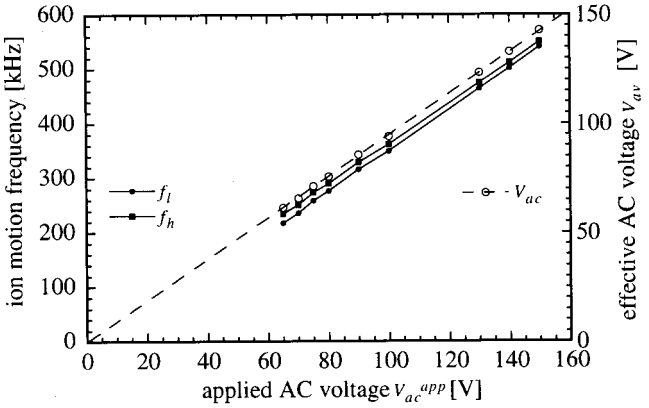

FIG. 7. Measured relation between the applied rf voltages V_{ac}^{app} and $f_{h,l}$. The slope of the dashed line yields the calibration relation from which the effective voltage is determined: $V_{ac}=0.95V_{ac}^{app}$ V. The trap operation parameters are $V_{dc}^{app}=0$, $\Omega/2\pi=7.04$ MHz, $B_0=0.004$ T.

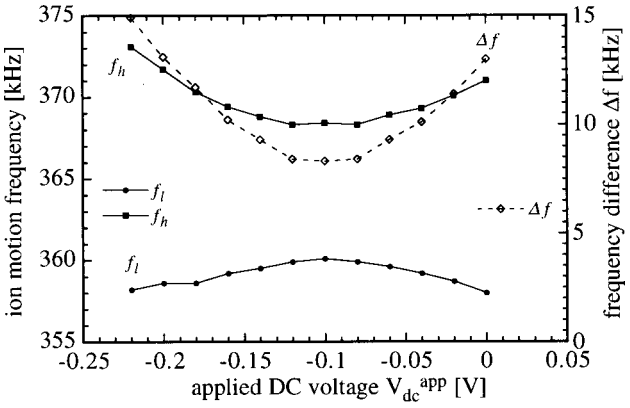

FIG. 8. Dependence of the ion oscillation frequencies and their difference on the applied V_{dc}^{app}. It can be estimated $V_{dc}=V_{dc}^{app}-0.1$ V for this particular experimental condition. The trap parameters are $V_{ac}^{app}=100$ V, $\Omega/2\pi=7.04$ MHz, $B_0=0.004$ T.

potential contribution, which arises when a minute beryllium film deposits on the trap electrodes during the laser ablation while loading the trap with ions. The extra loading section minimized this effect, but could not completely eliminate it. The calibration factors for the effective voltages were obtained by measuring the radial ion oscillation frequencies when the trap was operated at a negligibly weak magnetic field of $B=4\times10^{-3}$ T.

The calibration frequencies $f_{h,l}^0$ are the zero magnetic field intercepts displayed in Fig. 6(b) and were measured as a function of V_{ac}^{app} and V_{dc}^{app} as shown in Figs. 7 and 8, respectively. The q and a factors are obtained from the dependence of the average frequency $f_{av}=(f_h+f_l)/2\simeq\sqrt{2}q\Omega/8\pi$ and the difference frequency $\Delta f=f_h^0-f_l^0\simeq a\Omega^2/16\pi^2 f_{av}$. In this approximation, the variation of the closing voltage V_z over the trapped ion cloud can be neglected due to the smallness of the cloud. When inserted into Eq. (5) the effective voltages V_{ac} and V_{dc} follow. This procedure yields $V_{ac}=0.95V_{ac}^{app}$ V for our trap.

Figure 8 gives the relation $V_{dc}=V_{dc}^{app}-0.1$ V. The -0.1 V contribution is mainly due to the contact potential. Since the contact potential changes slowly over time periods of days, this value is not the same in all measurements. The small nonzero intercepts in Figs. 7 and 8 are due to the presence of a weak magnetic field and in Fig. 8 correspond with 8.3 kHz to the cyclotron frequency of $^9Be^+$ at 4×10^{-3} T.

V. SIMULATION OF THE ION MOTION DYNAMICS

The equation of the motion for a single $^9Be^+$ in a combined trap was also solved numerically. For the general case in which the magnetic field is inclined, $\mathbf{B}=B_0(\sin\theta\cos\phi,\sin\theta\sin\phi,\cos\theta)$, and inserting this into Eq. (3), the equations of motion become

$$\begin{aligned}
\ddot{x}&=-\frac{e}{mr_0^2}(V_{dc}-V_{ac}\cos\Omega t)x+\frac{e\alpha V_z}{mz_0^2}x\\
&\quad+\frac{eB_0}{m}(\dot{y}\cos\theta-\dot{z}\sin\theta\sin\phi),\\
\ddot{y}&=+\frac{e}{mr_0^2}(V_{dc}-V_{ac}\cos\Omega t)y+\frac{e\alpha V_z}{mz_0^2}y\\
&\quad+\frac{eB_0}{m}(\dot{z}\sin\theta\cos\phi-\dot{x}\cos\theta),\\
\ddot{z}&=-\frac{2e\alpha V_z}{mz_0^2}+\frac{eB_0}{m}(\dot{x}\sin\phi-\dot{y}\cos\phi)\sin\theta.
\end{aligned}\tag{20}$$

The small effect of the variation of V_z along the x, y coordinates can again be neglected. All results of the simulation were obtained using the same ion having an initial space coordinate (0.1, -0.1, -0.1) mm and energy value (0, 2.0, 1.0) meV.

A. Motion and frequencies in the *x*, *y* plane

After numerically finding the time evolution of the coordinates for a particular ion orbit by solving Eq. (20), the ion oscillation frequency spectrum was obtained by the FFT formalism. Figures 9(a) and 9(b) display examples of the calculated ion orbits together with their motional amplitudes for two different magnetic fields. The length of the central trap section was $2z_0=20$ mm, and the other parameters were $r_0=2.61$ mm, $\Omega/2\pi=8$ MHz, $V_{ac}=100$ V (V_z is neglected here). Figure 9(c) displays FFT spectra up to the second order. Depending on the operating parameters, ion orbits covering different regions around the trap center are readily recognized. The dominant strong zeroth order frequency components are readily seen. The amplitudes of the higher order n frequency components are smaller for slow ions and for the trapping parameters used. The higher order n frequencies follow the relation

$$\omega_{l,h}^n=\omega_{l,h}+n\Omega,\tag{21}$$

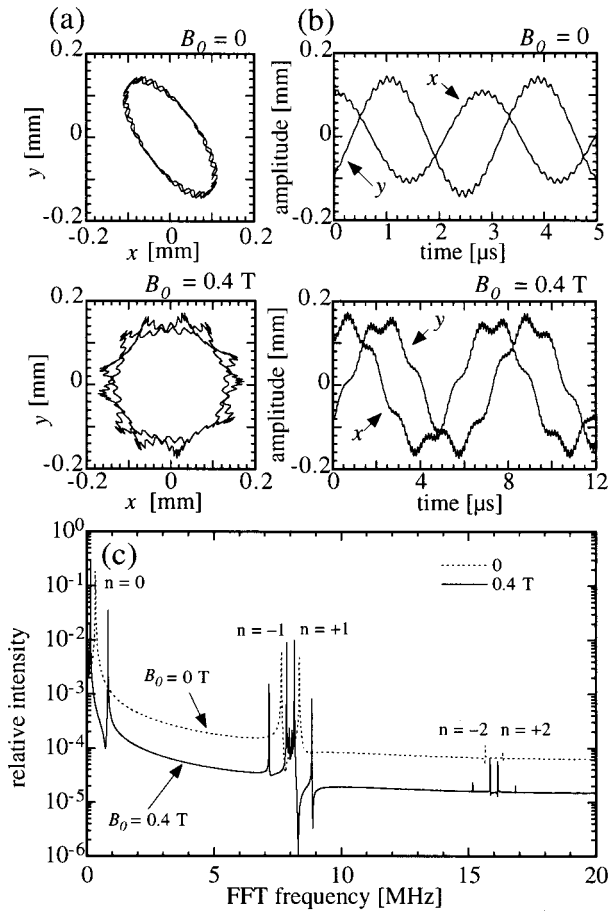

FIG. 9. (a) Ion orbits for two values of B_0 (0 and 0.4 T). (b) Corresponding ion motion amplitudes. (c) FFT spectra displaying the contribution of the zeroth, first, and second orders. ($V_{ac}=100$ V, $V_{dc}=0$, $\Omega/2\pi=8.0$ MHz, $\theta=\phi=0$, and V_z was neglected.)

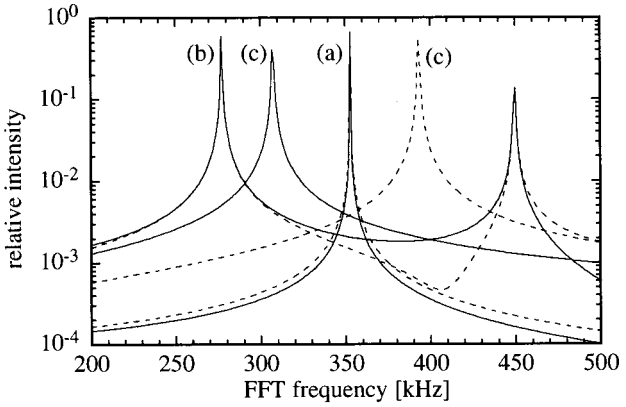

FIG. 10. FFT spectra of zeroth order displaying the splitting of the ion motion frequencies (solid line: x component, dashed line: y component). (a) Single line spectra for $V_{dc}=0$ and $B_0=0$. (b) Splitting into the two components f_l and f_h for $V_{dc}=0$ and $B_0=0.1$ T. (c) Splitting into two components x and y for $V_{dc}=0.75$ V and $B_0=0$. ($V_{ac}=100$ V, $\Omega/2\pi=8.0$ MHz, $\theta=\phi=0$, V_z was neglected.)

where we have set $\omega_{l,h}=2\pi f_{l,h}$. FFT spectra of the dominating zeroth order for various cases are depicted in Fig. 10. When the magnetic field is absent and $V_{dc}=0$ the two ion oscillation frequencies coincide (a). With increasing magnetic field the two motional frequencies split and are shifted toward higher and lower frequencies respectively (b). When $V_{dc}=0.75$ V, f_h and f_l are already split in the absence of a magnetic field (c). The splitting increases with V_{dc} and increases further as a function of increasing magnetic field.

VI. DISCUSSION OF THE RESULTS

Two theoretical approaches to calculate the ion oscillation frequencies have been described, and experimentally these frequencies have also been observed. In this section we compare the experimental results with the two theoretical calculations.

A. Comparison of experiment with the numerical simulation and the analytical solution

The magnetic field dependence of the radial macromotion frequencies f_h and f_l obtained by the various methods are shown in Fig. 11(a). The solid lines were calculated using the analytical solution of Eq. (14), the symbols give the results of the experiment and the numerical simulations. It can be seen that the results of the three methods give somewhat different values. The differences δf of the macromotion frequencies for the experimental and analytical values on one side with the simulation results on the other side are compiled for f_h in Fig. 11(b) and for f_l in Fig. 11(c) as a function of the magnetic field. The agreement is best between experiment and simulation.

Figure 12 indicates the contribution due to a nonzero bias voltage to the motional frequencies by plotting the frequency difference for $V_{dc}=0.75$ V and $V_{dc}=0$ versus magnetic field. It can be seen that for weak magnetic field ($B<0.2$ T), f_h and f_l have a strong dependence on V_{dc}, and that in the strong field region ($B>0.5$ T) f_h approaches the zero dc field value but f_l retains a small finite influence. This behavior is expected, since for f_h the magnetic field effect adds, but for f_l it subtracts from the motional frequencies without magnetic field.

In order to investigate where the approximate analytical solution deviates most from the more accurate simulation results we have plotted, in Fig. 13, the ion motion frequency difference δf for a fixed magnetic field as a function of the stability parameter q. δf_h is particularly large for large amplitudes V_{ac} of the driving field at frequency Ω, or more generally large values of the stability parameter q. This indicates the well known fact that the zeroth order solution results of the Mathieu equation are not sufficient for large values of V_{ac} or q and in this case the solutions of all order have to be employed simultaneously to get the correct result. For the case of large q the macromotion frequency f_h is no longer small compared with the driving frequency Ω and the cyclotron frequency f_c, and therefore the condition for the dominance of the zeroth order solution is no longer fulfilled. For the same reason δf is large for small values of Ω.

B. Motion and oscillation frequencies in the *z*-direction

In the experiment a dc bias voltage V_z is applied to the outer trap segments to confine the ions along the z direction.

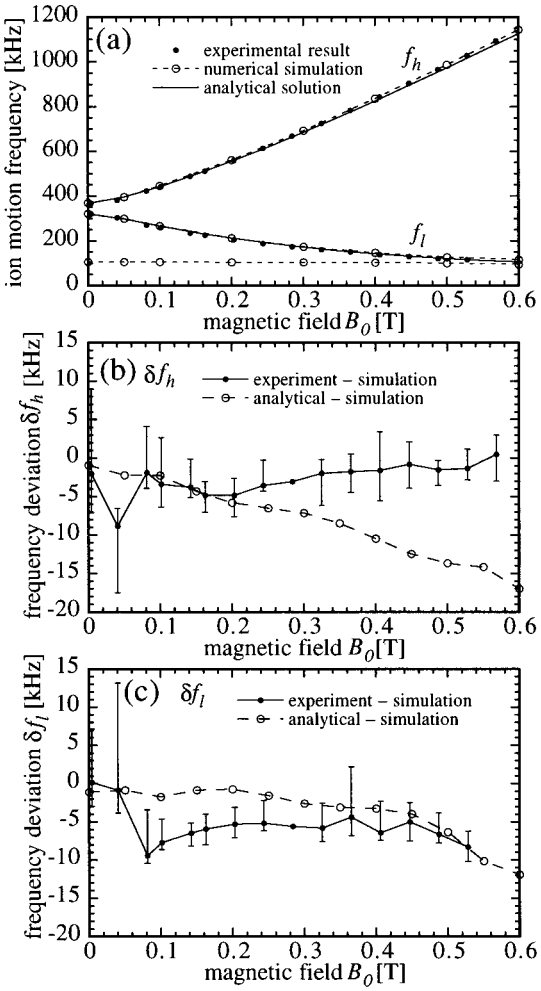

FIG. 11. (a) Field dependence of the ion motion frequencies observed by experiment and calculated in the numerical simulation and the analytical solution. (b) and (c) Comparison of the analytical results with the experimental and numerical FFT results. The deviation in ion motion frequencies $\delta f_{h,l}$ vs magnetic field is shown. (From the results in the present experiment we observed $f_h^0 \simeq 368$ kHz and $f_l^0 \simeq 320$ kHz at $B_0 = 0.004$ T, $V_{ac}^{app} = 100$ V, $\Omega/2\pi = 7.30$ MHz, $V_{dc}^{app} = 0$ and $V_z^{app} = 5$ V. It can be estimated that $V_{ac} = 95$ V, $V_{dc} = 0.43$ V, and $f_z(V_z) = 105$ kHz, therefore these values are used in the simulation and the analytical solution. In the simulation the inclination angles $\theta = 4°$ and $\phi = 45°$ were taken into consideration.)

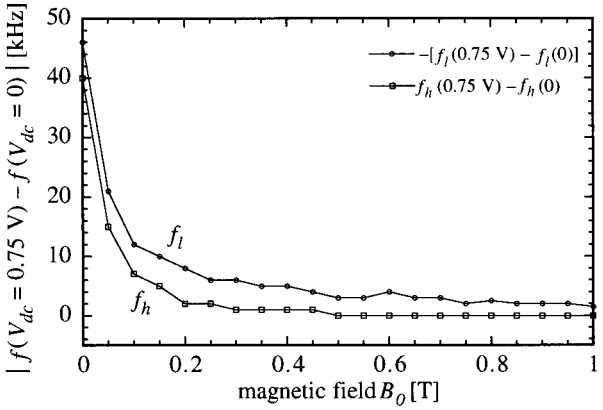

FIG. 12. Comparison of the numerical FFT results of $V_{dc} = 0.75$ V with $V_{dc} = 0$. ($V_{ac} = 100$ V, $\Omega/2\pi = 8.0$ MHz, $\theta = \phi = 0$, and V_z is neglected.)

In addition, in the present experimental arrangement, the trap electrodes were inclined at an angle θ of about 4° with respect to the direction of the magnetic field. In the following we have numerically calculated the effects of these conditions using Eq. (20). At the same time we have also observed them in the experiment. The results of the numerical simulation are shown in Fig. 14 for the angles $\theta = 4°$ and the trap operating parameters $V_{ac} = 100$ V, $V_{dc} = 75$ mV, $\Omega/2\pi = 6.63$ MHz, and $B = 0.4066$ T. The effect of the dc bias voltage V_z was included by setting $f_z(V_z) = 95$ kHz. The two frequencies f_l and f_z have similar values in the strong magnetic field since they are strongly coupled. We labeled the components of the corresponding two coupled frequencies f_{l1} and f_{l2}. They only appear when the magnetic field is inclined. There is also a dependence of the two coupled frequencies on V_{ac}. Figure 15(a) contains the experimental values of f_{l1} and f_{l2} measured for different values of V_{ac}. The simulation results are also indicated for the inclination angle $\theta = 4°$ of the magnetic field and agree well with the experimental results.

C. Spurious resonances

The identification of the observed resonances is made by their frequency values and their dependence on the operating parameters. In this context we have intermittently observed two series of weaker resonances at unexpected frequencies of about $\omega_h/3$ and $\omega_l/3$ [labeled f_h' and f_l' in Fig. 6(b)]. These resonances can be explained by the presence of impurity ions, which have a mass of about three times the beryllium mass and therefore are probably caused by Al^+ or Be_3^+ clusters. It should be noted that also f_l' coincides with f_{l1} of $^9Be^+$. The spurious resonances make themselves noticeable in the Be^+ fluorescence through sympathetic heating[28] of Be^+ ions by motionally excited impurity ions. In this process kinetic energy is transferred to the Be^+ ions from the resonantly excited impurity ions through Coulomb collisions. The sympathetic heating effect is largest when only a few single ions and a few impurity ions in the crystalline state are concentrated in close proximity near the ion trap axis. This is

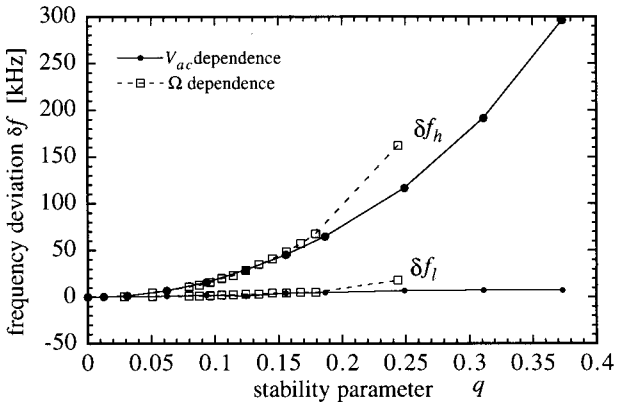

FIG. 13. Comparison of the numerical FFT results with the analytical results. The difference in calculated ion motion frequencies versus the stability parameter $q = q(V_{ac}, \Omega)$. (V_{ac} dependence: $V_{dc} = 0$, $\Omega/2\pi = 8.0$ MHz, $B_0 = 1$ T, $\theta = \phi = 0$. Ω dependence: $V_{ac} = 100$ V, $V_{dc} = 0$, $B_0 = 1$ T, $\theta = \phi = 0$.)

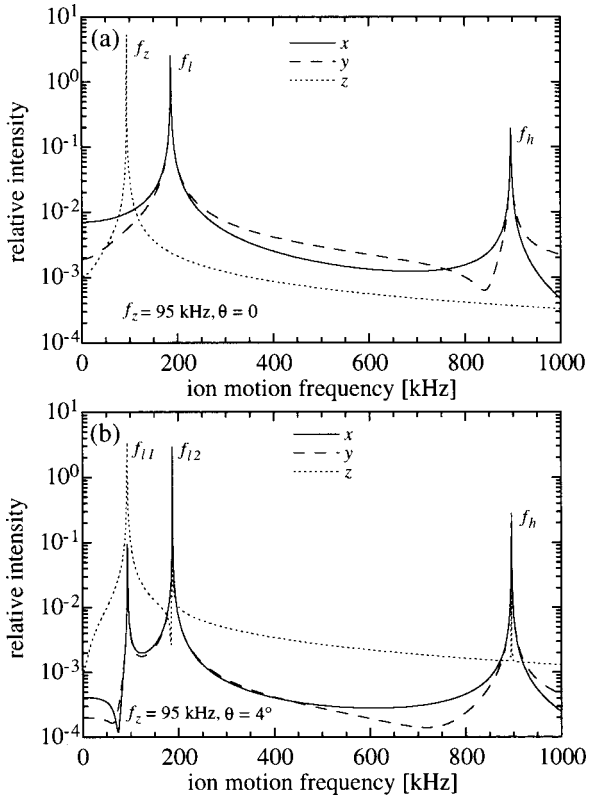

FIG. 14. (a) FFT spectra without inclination. (b) FFT spectra with the inclination angle $\theta=4°$. The motions of the *x*, *y*, and *z* directions are coupled. ($V_{ac}=100$ V, $V_{dc}=0$, $\Omega/2\pi=7.04$ MHz, $B_0=0.4066$ T, $\phi=45°$, and $f_z(V_z)=95$ kHz.)

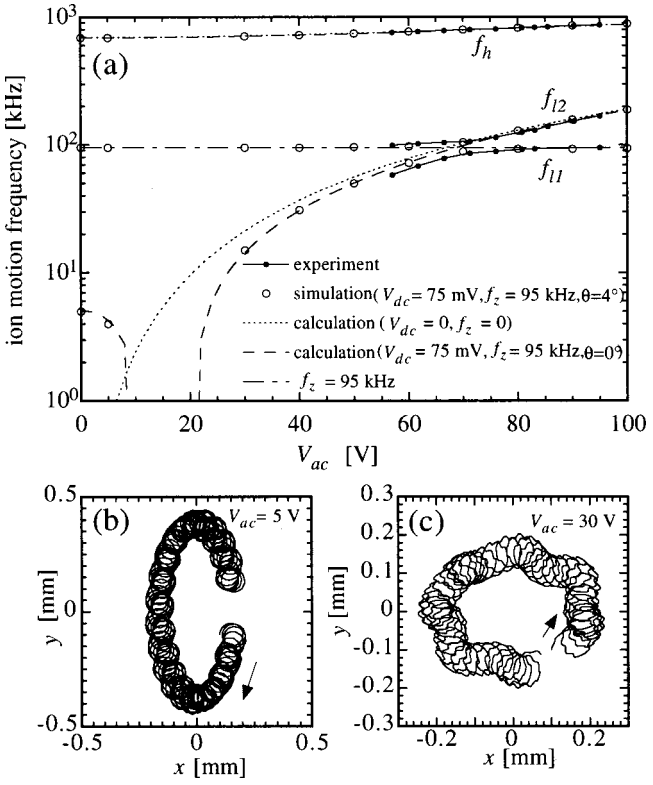

FIG. 15. (a) Measured and calculated inclination effect of the magnetic field on the f_{l1} and f_{l2} versus V_{ac}. Different ion trajectories (b) $V_{ac}=5$ V and (c) $V_{ac}=30$ V. Note that the rotational direction of ω_l changes. (Experiment: $V_{ac}=0.95V_{ac}^{app}$ V, $V_{dc}^{app}=0$, $\Omega/2\pi=6.63$ MHz, $B_0=0.4066$ T, $V_z^{app}=5$ V. Simulation: $\Omega/2\pi=6.63$ MHz, $V_{dc}=75$ mV, $B_0=0.4066$ T, $\theta=4°$, $\phi=45°$, $f_z=95$ kHz.)

evident from Fig. 6 where these resonances appear only in the lower traces when only a few ions are stored.

VII. MODES OF OPERATION

It is possible to operate the combined trap in two extreme regions, and instructive to consider these two cases in detail. Near zero magnetic field, the operation is close to that of a rf trap whereas near zero ac voltage the operation is close to that of a Penning trap. Earlier, for the case of the symmetrical trap[10] a particular example in which the magnetron motion vanishes has been discussed.[11] We have also studied these extreme regions of the linear combined trap. The measurements and results of the calculations are compiled in Fig. 16. The observations at near zero magnetic field demonstrate that in this limit the ion oscillation frequencies are made up of two harmonic oscillations about the trap center with a slow drift motion around the field lines superimposed on them, yielding and ω_l and ω_h. In addition f_z is the usual *z* motion. In this case the radial confinement is dominated by the rf fields. In the other extreme case of the near Penning trap mode, the low amplitudes V_{ac} of the driving rf field contribute very little to the radial trapping. We observed neither fluorescence nor motional resonances in this region. This fact can be explained by considering Fig. 15, which illustrated the results of a calculation. Similar to the case of the circular combined trap, there is an unstable region around the point where the direction of the magnetron rotation changes.[11] In our case, of the linear combined trap, the additional static quadrupole field in the radial direction due to the presence of a residual V_{dc} causes an even broader unstable region. In the present trap, typical values of the residual V_{dc} are about 100 mV. This fact makes even trap operation in the pure Penning trap mode difficult.

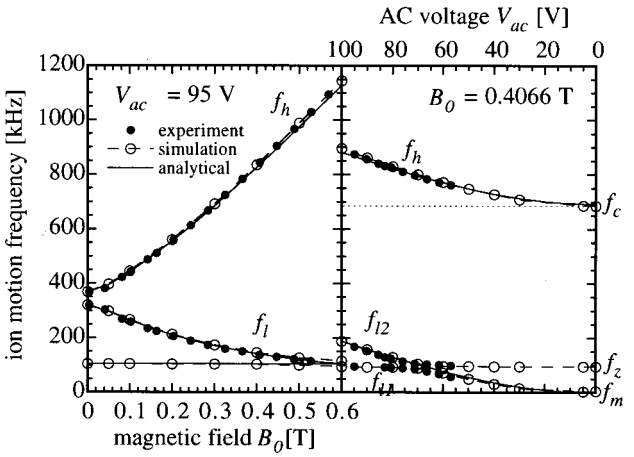

FIG. 16. Evolution of the ion motion frequencies with the magnetic field (left) and with the ac driving voltage (right). For zero magnetic field the Paul trap mode occurs. For zero ac voltage the near Penning trap results [Note the different maximum values of the magnetic field, which is $B_{max}=0.6$ T (left) and $B_0=0.4066$ T (right)].

VIII. SUMMARY

We have demonstrated a trapping technique that is particularly well suited for catching externally generated ions. The analytical and numerical models explain the observed oscillation frequencies. The importance of the coupling of the various degrees of freedom of the ion motion is reflected by the shifts of the oscillation frequencies in the different magnetic field regions, in the various modes of operation, and the possible orientations of the magnetic field.

ACKNOWLEDGMENTS

The authors acknowledge valuable discussions with X. Zhao and G. Agnolet.

[1] W. Paul, O. Osberghaus, and E. Fischer, Forschungsber. Wirtsch. Verkehrsministeriums Nordrhein-Westfalen , 45 (1958).
[2] E. Fischer, Z. Phys. **156**, 1 (1958).
[3] H. G. Dehmelt, Adv. At. Mol. Phys. **3**, 53 (1967); **4**, 109 (1969).
[4] H. A. Schuessler, E. N. Fortson, and H. G. Dehmelt, Phys. Rev. **187**, 5 (1969).
[5] F. M. Penning, Physica (Amsterdam) **3**, 873 (1936).
[6] L. S. Brown and G. Gabrielse, Rev. Mod. Phys. **58**, 233 (1986).
[7] H. G. Dehmelt and F. Walls, Phys. Rev. Lett. **21**, 127 (1968).
[8] C.-S. O and H. A. Schuessler, J. Appl. Phys. **52**, 2601 (1981).
[9] G. Z. Li, Z. Phys. D: At., Mol. Clusters **10**, 451 (1988).
[10] D. J. Bate, K. Dholakia, R. C. Thompson, and D. C. Wilson, J. Mod. Opt. **39**, 305 (1992).
[11] K. Dholakia, G. Zs. K. Horvath, D. M. Segal, and R. C. Thompson, J. Mod. Opt. **39**, 2178 (1992).
[12] G. Zs. K. Horvath, J. L. Hernandez-Pozos, J. Rink, D. M. Segal, and R. C. Thompson, Phys. Rev. A **57**, 1944 (1998).
[13] M. Yan, X. Luo, and X. Zhu, Appl. Phys. B: Lasers Opt. **67**, 235 (1998).
[14] M. G. Raizen, J. M. Gilligan, J. C. Bergquist, W. M. Itano, and D. J. Wineland, Phys. Rev. A **45**, 6493 (1992).
[15] M. Welling, H. A. Schuessler, D. J. Wineland, R. I. Thompson, and H. Walther, Int. J. Mass Spectrom. Ion Processes **172**, 95 (1998).
[16] H. A. Schuessler, E. C. Benck, and J. Lassen, Hyperfine Interact. **81**, 263 (1993).
[17] M. Wada, I. Katayama, H. Kawakami, J. Tanaka, S. Fujitaka, Y. Ogino, H. Wang, K. Okada, T. Nakamura, and S. Ohtani, Hyperfine Interact. **103**, 59 (1996).
[18] K. Okada, M. Wada, H. Wang, T. Nakamura, S. Fujitaka, J. Tanaka, H. Kawakami, S. Ohtani, and I. Katayama, Phys. Scr., T **73**, 67 (1997).
[19] M. Wada, K. Okada, H. Wang, K. Emders, L. Kurth, T. Nakamura, S. Fujitaka, J. Tanaka, H. Kawakami, S. Ohtani, and I. Katayama, Nucl. Phys. A **626**, 365c (1997).
[20] K. Okada, M. Wada, T. Nakamura, R. Iida, S. Ohtani, J. Tanaka, H. Kawakami, and I. Katayama, J. Phys. Soc. Jpn. **67**, 3073 (1998).
[21] W. M. Itano and D. J. Wineland, Phys. Rev. A **24**, 1364 (1981).
[22] J. J. Bollinger, J. D. Prestage, W. M. Itano, and D. J. Wineland, Phys. Rev. Lett. **54**, 1000 (1985).
[23] S. Fujjitaka *et al.*, Nucl. Instrum. Methods Phys. Res. B **126**, 386 (1997).
[24] H. A. Schuessler, Phys. Today **34**, 48 (1981).
[25] A. Bohr and V. F. Weisskopf, Phys. Rev. **77**, 94 (1950).
[26] N. W. McLachlan, in *Theory and Applications of Mathieu Functions* (Clarenden Press, Oxford, 1947).
[27] C.-S. O and H. A. Schuessler, Int. J. Mass Spectrom. Ion Processes **35**, 305 (1980).
[28] D. J. Larson, J. C. Bergquist, J. J. Bollinger, W. M. Itano, and D. J. Wineland, Phys. Rev. Lett. **57**, 70 (1986).